JGR Biogeosciences

RESEARCH ARTICLE
10.1029/2019JG005487

Coupled Nitrate and Phosphate Availability Facilitated the Expansion of Eukaryotic Life at Circa 1.56 Ga

Zhipeng Wang[1], Xinqiang Wang[1,2], Xiaoying Shi[1,2], Dongjie Tang[2,3], Eva E. Stüeken[4,5], and Huyue Song[6]

[1]School of Earth Sciences and Resources, China University of Geosciences (Beijing), Beijing, China, [2]State Key Laboratory of Biogeology and Environmental Geology, China University of Geosciences (Beijing), Beijing, China, [3]Institute of Earth Sciences, China University of Geosciences (Beijing), Beijing, China, [4]School of Earth and Environmental Sciences, University of St Andrews, St Andrews, UK, [5]NASA Astrobiology Institute, Virtual Planetary Laboratory, University of Washington, Seattle, WA, USA, [6]State Key Laboratory of Biogeology and Environmental Geology, China University of Geosciences, Wuhan, China

Key Points:
- Integrated data of $\delta^{15}N$, $\delta^{13}C_{org}$, and major and trace element contents are reported from the circa 1.56 Ga Gaoyuzhuang Formation in North China
- The preservation of an aerobic N cycling signal in a stratified ocean is attributed to joint effects of O_2 rise and low primary productivity
- The evolutionary leap of eukaryotes at circa 1.56 Ga was triggered by expanding reservoirs of multiple essential nutrients

Supporting Information:
- Supporting Information S1

Correspondence to:
X. Wang and X. Shi,
wxqiang307@126.com;
shixyb@cugb.edu.cn

Citation:
Wang, Z., Wang, X., Shi, X., Tang, D., Stüeken, E. E., & Song, H. (2020). Coupled nitrate and phosphate availability facilitated the expansion of eukaryotic life at circa 1.56 Ga. *Journal of Geophysical Research: Biogeosciences*, *125*, e2019JG005487. https://doi.org/10.1029/2019JG005487

Received 24 SEP 2019
Accepted 17 MAR 2020
Accepted article online 19 MAR 2020

Abstract Recent geochemical and paleontological studies have revealed a significant ocean oxygenation episode and an evolutionary leap of eukaryotes at the onset of the Mesoproterozoic. However, the potential role of nitrogen availability and its interaction with other nutrients in these environmental and biological events have not been investigated. Here we present an integrated study of nitrogen isotopes ($\delta^{15}N$), organic carbon isotopes ($\delta^{13}C_{org}$), and major and trace element concentrations from Member III of the Gaoyuzhuang Formation in the central North China Craton where the earliest macroscopic multicellular eukaryotic fossils were reported. The enrichments of redox-sensitive elements (Mo, U, and V), coupled with Mo-U covariations, $\delta^{13}C_{org}$, and I/(Ca + Mg), indicate that the Gaoyuzhuang Member III in the study area was deposited in largely suboxic-anoxic environments with ephemeral occurrences of euxinia. These data reinforce previous inferences of a strongly redox stratified ocean during the early Mesoproterozoic, but a pulsed oxygenation event may have resulted in deepening of the chemocline. The high $\delta^{15}N$ values from the study section are interpreted as a result of aerobic N cycling and the presence of a fairly stable nitrate pool in the surface oxic layer, possibly due to the combined effects of oxygenation and low primary productivity. Increased availability of nitrate could have contributed to the expansion of eukaryotic life at this time. However, our data also suggest that nitrate alone was not the only trigger. Instead, this evolutionary leap was likely facilitated by multiple environmental factors, including a rise in O_2 levels and increasing supplies of phosphorus and other bio-essential trace elements.

Plain Language Summary The oldest macroscopic eukaryotes (algae) first appeared in ancient oceans about 1.56 billion years ago. Before that, only simple and microscopic fossils have been discovered. The reason behind this evolutionary leap is, however, still puzzling scientists. Here we use multiple proxies to study the change of nutrient and oxygen levels during this critical period. Our results demonstrate the availability of the nutrient nitrogen (in form of nitrate) in the oxic surface ocean owing largely to restrictive consumption by organic carbon decomposition, providing favorable N substance for bio-utilization. Furthermore, we also found evidence for the joint increase of O_2 level, seawater phosphorus, and some bio-essential trace elements along with the occurrence of these earliest algae. Our study provides important clues for untangling the triggers of biological innovation at circa 1.56 Ga.

1. Introduction

Following their first emergence in the Paleoproterozoic or even earlier, the evolution of eukaryotes during the succeeding Mesoproterozoic was remarkably slow (e.g., Knoll, 2014; Javaux & Lepot, 2018). Although recent paleontological studies suggest a preliminary development of eukaryotes in the late Paleoproterozoic to early Mesoproterozoic (~1.8–1.5 Ga) (Miao et al., 2019; Shi et al., 2017; Zhu et al., 2016), their abundance and diversity remained low until the late Neoproterozoic. This evolutionary stasis has long been linked to low oxygen concentrations in the atmosphere-ocean system (e.g., Lyons et al., 2014; Reinhard et al., 2016), based on several lines of geochemical evidence, including redox sensitive element (RSE) contents in sedimentary rocks (Partin et al., 2013; Reinhard et al., 2013; Robbins et al., 2016;

Sahoo et al., 2012; Scott et al., 2008; Sheen et al., 2018), iron speciation (Li et al., 2015; Planavsky et al., 2011; Poulton & Canfield, 2011; Sperling et al., 2015), chromium isotope ($\delta^{53}Cr$) records in ironstones and in fine-grained siliciclastic rocks (Cole et al., 2016; Planavsky et al., 2014), cerium anomalies (Tang et al., 2016), carbon and sulfur isotope compositions (Gilleaudeau & Kah, 2015; Guo et al., 2013; Luo et al., 2014, 2015), ratios of iodine-to-calcium–magnesium [I/(Ca + Mg)] (Hardisty et al., 2017; Shang et al., 2019), and zinc-to-iron (Zn/Fe) ratios (Liu et al., 2016) in carbonate rocks. Importantly, expanded ocean anoxia during the Mesoproterozoic could have resulted in nitrogen (N) limitation (Anbar & Knoll, 2002) through substantial fixed N loss by denitrification and anammox, analogous to modern redox stratified basins (Ader et al., 2016; Fennel et al., 2005). This hypothesis is supported by nitrogen isotope ($\delta^{15}N$) studies from three Mesoproterozoic basins in the United State and in Australia (Koehler et al., 2017; Stüeken, 2013). In addition, enhanced phosphorus (P) scavenging in the anoxic, iron rich Mesoproterozoic ocean may have reduced P availability (Derry, 2015; Reinhard et al., 2017; Zegeye et al., 2012). The scarcity of macronutrient elements (N or P, or both) could have limited the rate of primary productivity in the ocean, which, in turn, may have delayed eukaryotic evolution (Anbar & Knoll, 2002; Fennel et al., 2005; Reinhard et al., 2017, 2020).

Although, on average, atmospheric oxygen levels may have been relatively low in the Mesoproterozoic compared to modern levels, the Mesoproterozoic ocean appears to have experienced several pulses of oxygenation. For instance, the circa 1.4 Ga black shale of Unit 3 of the Xiamaling Formation in North China shows enrichments in molybdenum (Mo) and uranium (U) but depletion or nonenrichment in vanadium (V) relative to average continental crust, which was interpreted as an indicator of oxygenated bottom waters (Zhang et al., 2016; but see alternative views in Planavsky et al., 2016, and Scholz, 2018). A numerical model of the marine carbon-oxygen cycle suggests that these data require atmospheric oxygen level of >4% of present-day levels (PALs) (Zhang et al., 2016). The signals of an oxygen rise at circa 1.4 Ga have also been captured by integrated geochemical data from the Arlan Member of the Kaltasy Formation, central Russia (Sperling et al., 2014); the presence of jasper related to deep marine volcanogenic massive sulphide deposits (Slack et al., 2007); the U isotope ($\delta^{238}U$) records from black shales of the Velkerri Formation in the Roper Basin, Australia (Yang et al., 2017); and by highly fractionated $\delta^{53}Cr$ in anoxic black shale (with negative Ce anomaly) of the Shengnongjia Group, South China (Canfield et al., 2018). A potential consequence of this oxygen rise could be an elevated supply of nitrate (NO_3^-) through nitrification and aerobic N cycling at least in the onshore areas, as evidenced by high $\delta^{15}N$ values documented from the Belt basin of the USA (Stüeken, 2013) and from the Bangemall and Roper basins of Australia (Koehler et al., 2017).

Another important period of temporary oxygenation may have occurred in the early Mesoproterozoic. Supporting evidence comes from the circa 1.60–1.54 Ga Gaoyuzhuang Formation (Lu et al., 2008; Li et al., 2010), North China. Recently, Zhang et al. (2018) reported an integrated study of rare earth elements (REEs), Fe speciation, and inorganic carbon isotopes ($\delta^{13}C_{carb}$) from the Gaoyuzhuang Formation. The moderately negative Ce anomalies in the Member III of the Gaoyuzhuang Formation were interpreted as an imprint of significant oxygenation at circa 1.56 Ga. A negative $\delta^{13}C_{carb}$ excursion in the lower part of Member III was attributed to the oxidation of ^{13}C-depleted organic carbon in response to the oxygen rise (Zhang et al., 2018). Importantly, this inferred oxygenation event at circa 1.56 Ga is broadly coincident with the early diversification of eukaryotes and the occurrence of decimeter-scale multicellular eukaryotes (Shi et al., 2017; Zhu et al., 2016), suggesting a possible causal link between them.

A key question that has not yet been investigated is what role the nitrogen cycle and/or its interaction with other nutrients may have played in the environmental turnover and biological innovation at circa 1.56 Ga. In this paper, we present integrated data of $\delta^{15}N$, $\delta^{13}C_{org}$, and major and trace element contents from Member III of the Gaoyuzhuang Formation. The $\delta^{15}N$ in sedimentary rocks can be used as an effective proxy for N cycling and ocean redox conditions in deep time because N is redox sensitive and displays characteristic isotopic fractionations during redox transformations (e.g., Ader et al., 2016; Stüeken et al., 2016; Wang, Jiang, et al., 2018; Wang, Ling, et al., 2018; Zerkle et al., 2017). Our new data along with previously published geochemical and paleontological data from time-equivalent strata (e.g., Guo et al., 2013; Luo et al., 2014; Shang et al., 2019; Tang et al., 2016; Zhang et al., 2018) provide comprehensive insights into linkages between the oceanic N cycle, ocean redox conditions, and eukaryote evolution.

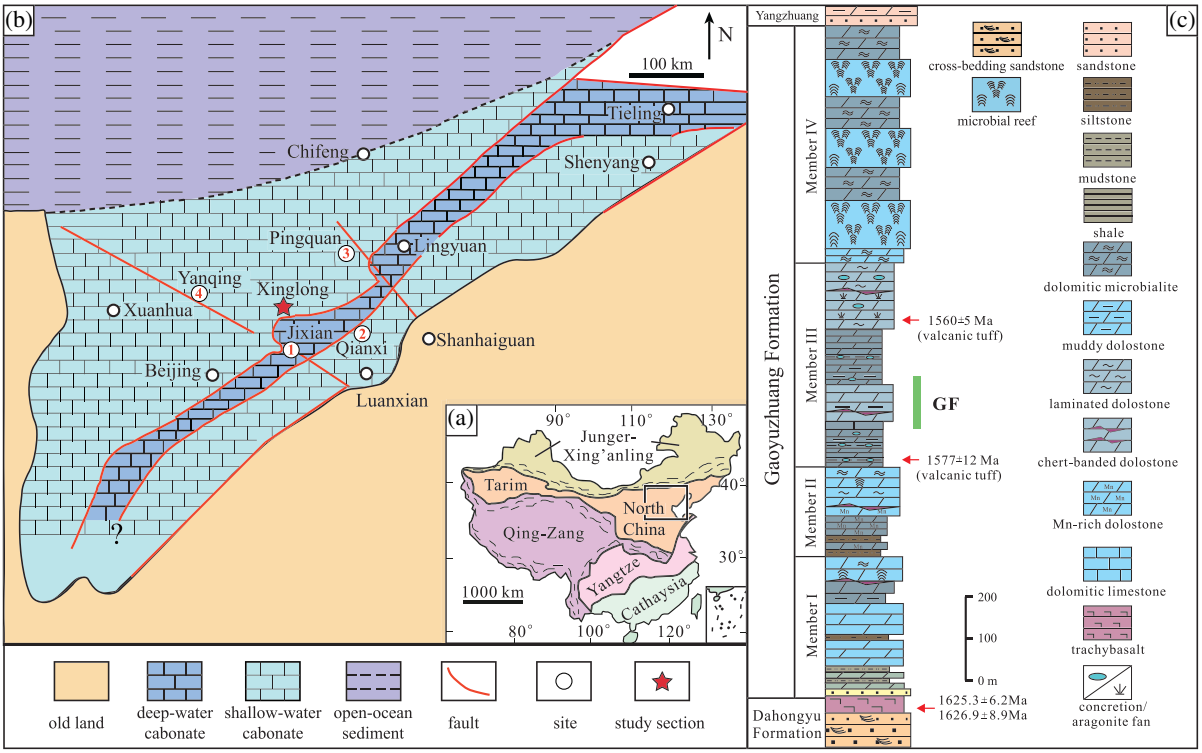

Figure 1. Paleogeographic maps and generalized stratigraphic column of the Gaoyuzhuang Formation in the central North China Platform. (a) Tectonic outline showing the location of the North China Craton. The black square marks the position of the Yanliao Basin. (b) Paleogeography during the deposition of the Gaoyuzhuang Formation, modified from Qiao and Gao (2007) and Qiao et al. (2007). The red star shows the location of the study section; the circled numbers refer to other sections discussed in this paper: (1) Jixian section, (2) Qianxi section, (3) Pingquan section, and (4) Yanqing section. (c) Generalized stratigraphic column of the Gaoyuzhuang Formation in the stratotype section at Jixian, Tianjin. The ages are adopted from Lu and Li (1991), Gao et al. (2008), and Li et al. (2010), the occurrence of the Gaoyuzhuang fossils refers to Zhu et al. (2016).

2. Geological Background and Sampling

The Gaoyuzhuang Formation, the basal unit of the Jixian Group unconformably overlying the Dahongyu Formation, is widespread and well preserved in the Yanliao Basin on the central North China Craton (Figure 1a). Paleogeographic reconstructions and sedimentological studies show that this formation is lithologically dominated by shallow-water carbonates, ranging from supratidal to deep subtidal facies, that were deposited in an epeiric sea (Figure 1b; Qiao & Gao, 2007; Qiao et al., 2007; Tang et al., 2016). In the stratotype section of the Jixian area, northern Tianjin, the Gaoyuzhuang Formation is traditionally subdivided into four lithostratigraphic members (Figure 1c) that are regionally traceable across the basin. Member I consists mainly of dolostones, silicified dolomicrite, and stromatolitic dolostone with subordinate sandstone and siltstone in the lower to middle part. Ripple marks and cross-bedding are observed in this member, suggestive of supratidal to shallow subtidal deposition. The age of the basal Member I is circa 1600 Ma (Tang et al., 2016), according to zircon U-Pb ages of 1625 ± 6 Ma (Lu & Li, 1991), 1622 ± 23 Ma (Lu et al., 2008), and 1626 ± 9 Ma (Gao et al., 2008) obtained from volcanic rocks in the upper part of the underlying Dahongyu Formation and a zircon U-Pb age of 1577 ± 12 Ma (Tian et al., 2015) from the middle part of the Gaoyuzhuang Formation. Member II is mainly composed of medium-bedded Mn-rich argillaceous dolomicrite, dolomitic siltstone, and thick-bedded dolostone, which were likely deposited in subtidal environments. The lower part of Member III is characterized by thin to medium bedded muddy dolostone and dolomitic limestone with interbedded black shale, which contain abundant carbonate concretions and diverse microscopic and macroscopic eukaryotes (Shi et al., 2017; Zhu et al., 2016). A U-Pb age of 1577 ± 12 Ma has been reported from a tuff layer in the lower part of this interval (Tian et al., 2015). The upper part of Member III is dominated by medium to thick bedded dolostone and dolomitic limestone with well-preserved molar tooth structures. Two identical zircon U-Pb ages of 1559 ± 12 Ma and 1560 ± 5 Ma were reported from a tuff bed within this

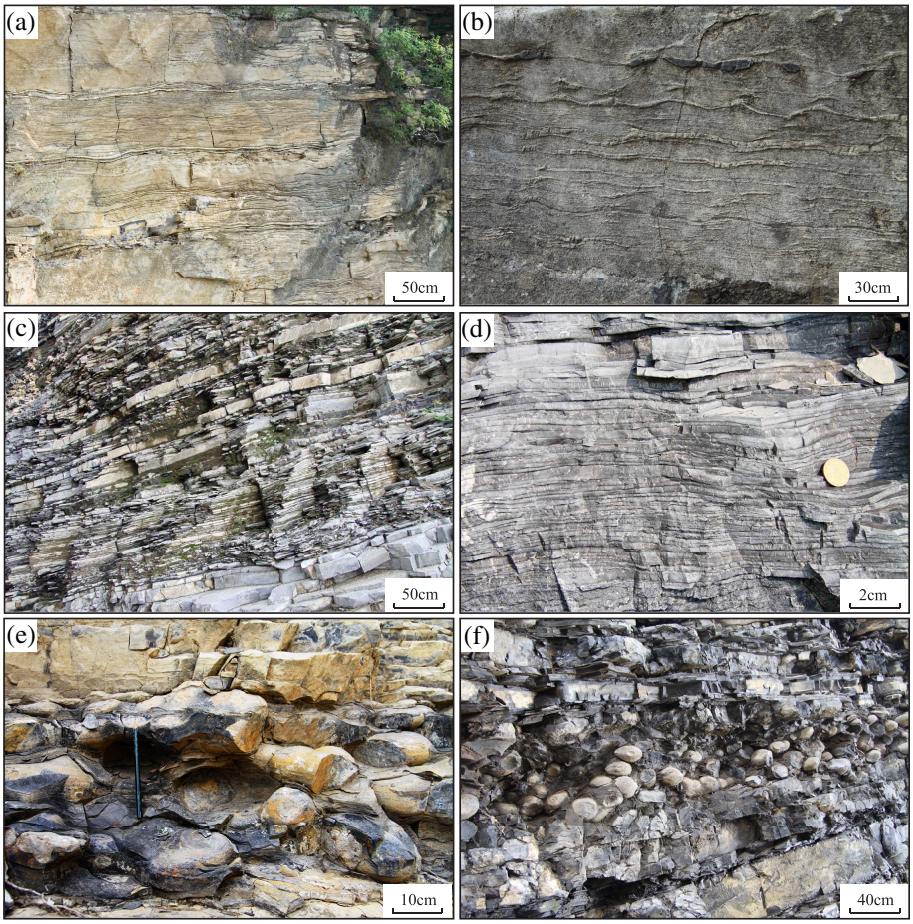

Figure 2. Macroscopic features of the Gaoyuzhuang Formation in the studied section. (a) Dolomitic microbialite with fine laminations from the upper part of Member II; (b) dolostone with cherty bands in the upper part of Member II; (c) thin- to medium-bedded limestone with intercalated calcareous mudstone and shale in Member III; (d) close-up view of thin-bedded limestone in Member III; and (e and f) fist-sized carbonate concretions in Member III.

interval in the Yanqing area, northwestern Beijing (Li et al., 2010). Overall, Member III is interpreted to represent a large transgression-regression cycle (Mei, 2005). The maximum water depth is probably reflected by the lower part of Member III, which was likely deposited close to storm wave base (Tang et al., 2016). Member IV is characterized by massive reefal microbialites alternating with thick-bedded cherty dolostone. In the Yanqing area (Shang et al., 2019; Tang et al., 2016) and Pingquan area (Guo et al., 2013; Guo et al., 2015), densely packed stromatolite columns up to 1.8 m long and 35 cm wide are observed in this unit. They form massive reef framestones composed typically of multibranching stromatolites and variably shaped thrombolites with well-developed herringbone calcite patches as pore-filling precipitates (Tang et al., 2017). No radiometric age has been reported for Member IV, but based on the two zircon U-Pb ages of 1483 ± 13 Ma and 1487 ± 16 Ma from the middle part of the overlying Wumishan Formation (Su, 2014), the top of the Gaoyuzhuang Formation most likely falls around circa 1540 Ma (Shang et al., 2019; Tang et al., 2016).

Our samples were collected from the Xinglong section (40°25′43.20″N, 117°54′06.69″E), about 60 km north to the Jixian section (Figure 1b). In this section, the Gaoyuzhuang Formation is only partially exposed, including the upper part of Member II and the lower-middle part of Member III. The upper Member II is dominated by medium- to thick-bedded Mn-bearing dolostone, dolomitic microbialite, and cherty dolostone with well-developed microbial laminae (Figures 2a and 2b). The overlying Member III consists mainly of thin- to medium-bedded dolomicrite, dolomitic limestone, and marl intercalated with calcareous mudstone and shale (Figures 2c, 2d, 3a, and 3b). The boundary between the Members II and III is marked with a clear

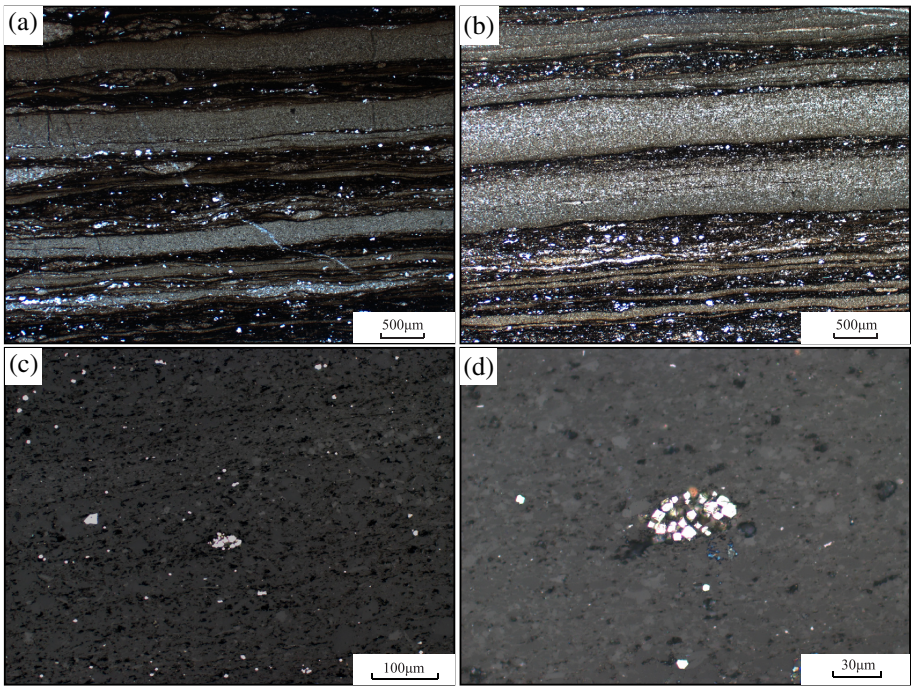

Figure 3. Microscopic features of Gaoyuzhuang Member III in the studied section. (a) Transmitted light image showing interbedded limestone and organic-rich mudstone; (b) transmitted light image showing argillaceous limestone with horizontal laminations; (c) reflected light image showing abundant disseminated pyrite in mud matrix; and (d) reflected light image showing pyrite aggregates in mud matrix.

flooding surface and occurrences of carbonate concretions. This horizon can be well correlated with the equivalent bed in the stratotype section at Jixian and in the other sections at Yanqing and Pingquan (Guo et al., 2013; Shang et al., 2019). Abundant fist-sized carbonate concretions are observed in the lower part of the Member III (Figures 2e and 2f). The general absence of wave- and current-influenced depositional structures and overall fine-grained sediments with horizontal bedding (Figures 2a, 3a, and 3b) in this member indicate a depositional environment below fair wave base, possibly around storm wave base. Disseminated and aggregated euhedral pyrites are observed in the mudstone interbeds (Figures 3c and 3d). The studied samples were mainly collected from fresh mudstone, shale, and marl in Member III, which are sufficiently enriched in organic matter and nitrogen to perform nitrogen isotope analyses.

3. Analytical Methods

3.1. Major and Trace Element Concentrations

Major element concentrations were analyzed at China University of Geosciences (Beijing) (CUGB) using a handheld energy dispersive XRF spectrometer (HHXRF) on sample powers below 200 mesh. A reference material (GSR-5) with known values was measured after every five samples. The analytical uncertainties for major elements are generally ≤10%. For trace element analyses, the samples were prepared following a traditional multistep acid digestion procedure. First, sample powders of ~25 mg were treated with 1.5 ml concentrated HF and 0.5 ml concentrated HNO_3 and heated in an oven at 220 °C for 24 hr. Subsequently, the samples were evaporated to near dryness on a hotplate and then dissolved in 0.5 ml concentrated HNO_3. These drying and dissolving processes were repeated three times. Thereafter, the samples were redissolved in a 2.5 ml mixed solution (1:1) of concentrated HNO_3 and deionized water and heated again in an oven at 150 °C for 4 hr. Finally, the solution was decanted into a polyethylene bottle and diluted 1,000-fold by ultrapure water before element analyses. Trace element concentrations were analyzed at the National Research Center for Geoanalysis, Chinese Academy of Geological Sciences (CAGS) using a PerkinElmer NexION 300Q inductively coupled plasma mass spectrometer (ICP-MS). Rh and Re were used

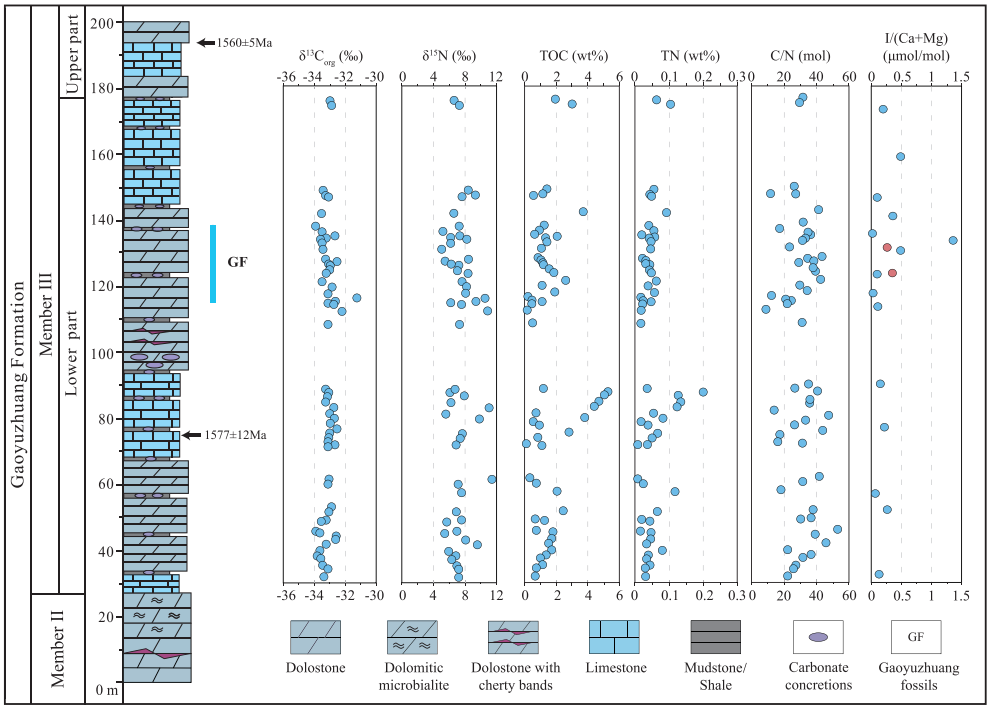

Figure 4. Organic carbon isotope, nitrogen isotope and I/(Ca + Mg) profiles in Gaoyuzhuang Member III of the Xinglong section. Red circles indicate I/(Ca + Mg) from carbonate concretions.

as internal standards. Reference materials of the National Research Center for Geoanalysis (GSR5) were used to monitor analytical uncertainties, which are better than 10% for most of elements.

3.2. I/(Ca + Mg)

Fresh chips of 17 carbonate samples were ground into powders below 200 mesh for I analyses following previously described procedures (Hardisty et al., 2017; Shang et al., 2019; Wei et al., 2019). Briefly, sample powders of ~40 mg were ultrasonicated in ultrapure water for 2 hr and then centrifuged. The water was discarded. Subsequently, the washed powders were treated with 3% HNO_3 to allow complete dissolution of carbonates. After further sonication and centrifugation, 0.5% tertiary amine was added to the supernatant to stabilize iodine (Hardisty et al., 2017; Lu et al., 2010). The iodine concentrations were measured using an Agilent 7500ce inductively coupled plasma mass spectrometer (ICP-MC) at the National Institute of Metrology, China. Analytical uncertainties monitored by the reference standard GSR 12 (I content, 0.23 μg/g) and duplicate samples are better than 10%. Magnesium and calcium contents were measured using a HHXRF at China University of Geosciences (Beijing). Using GSR-12 as the standard for Mg (Mg content, 13.14%) and Ca (Ca content, 21.44%), the analytical uncertainty was ≤10% for both Mg and Ca.

3.3. Nitrogen Isotope and Organic Carbon Isotope Compositions

Nitrogen isotope compositions ($\delta^{15}N$) were analyzed for 60 samples from organic-rich calcareous mudstone, shale, and argillaceous limestone at the State Key Laboratory of Biogeology and Environmental Geology, China University of Geosciences (Wuhan) (CUG), following previously described procedures (Xu et al., 2020). Fresh sample chips without any weathering surface and visible veins were ground into powders below 200 mesh in an agate mortar. Aliquots of sample powders were treated with 5% HCl to remove carbonate. The residue was rinsed with deionized water and centrifuged repeatedly until the pH reached a nearly neutral value. Thereafter, the samples were dried in an oven and then weighed into tin capsules for isotopic analyses. The $\delta^{15}N$ compositions were analyzed using an elemental analyzer (EA) connected to a Delta V mass spectrometer and are reported in standard δ notation in per mil (‰) deviations from atmospheric N_2 (‰, Air). Every five samples were followed by two international standards USGS40 ($\delta^{15}N = -4.52 \pm 0.06$‰) and

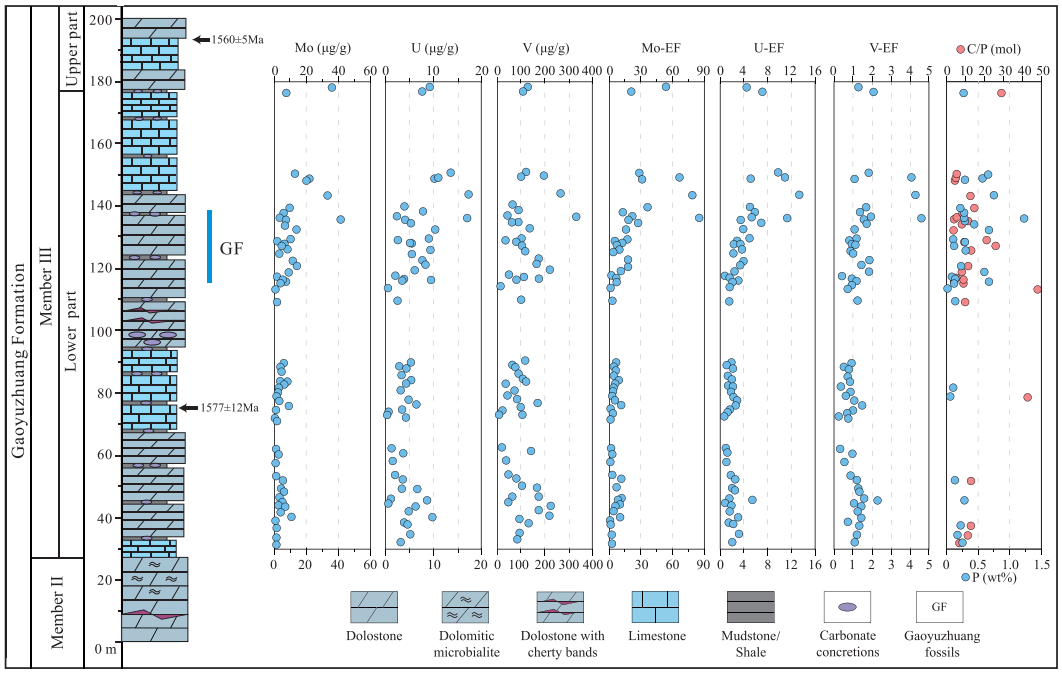

Figure 5. Variations of RSEs concentrations, enrichment factors, P contents, and molar C/P ratios in Gaoyuzhuang Member III of the Xinglong section.

IAEA-N-2 ($\delta^{15}N = +20 \pm 0.2‰$). A parallel sample was inserted after every 10 samples. Analytical uncertainties expressed as standard deviations of the repeated analyses of references were better than 0.2‰.

Organic carbon isotope compositions ($\delta^{13}C_{org}$) were measured on the same sample powders used for $\delta^{15}N$ analyses at the Laboratory for Stable Isotope Geochemistry, Institute of Geology and Geophysics, Chinese Academy of Sciences (IGGCAS). The decarbonation method is similar to that applied for $\delta^{15}N$ measurements described above. The $\delta^{13}C_{org}$ analyses were performed using an EA coupled to a MAT-253 mass spectrometer. Isotopic values are reported in per mil (‰) relative to the Vienna Pee Dee Belemnite (VPDB) standard. Analytical uncertainties monitored by the two internal laboratory standards GSW 04407 ($\delta^{13}C = -22.43 \pm 0.07‰$) and GBW04408 ($\delta^{13}C = -36.91 \pm 0.10‰$) were better than 0.15‰.

3.4. TOC and TN Contents

For TOC and TN analyses, aliquots of sample powders were decarbonated with 5% HCl, the residue was washed by deionized water and dried repeatedly to achieve a nearly neutral pH value. TOC and TN contents were analyzed at CUGB using an Elementer Macro Cube element analyzer. The relative analytical uncertainties are <0.5%.

4. Results

The $\delta^{15}N$, $\delta^{13}C_{org}$, TOC, TN, and C/N values are shown in Figure 4 and Table S1 in the supporting information. The $\delta^{15}N$ values in the study section vary from +4.62‰ to +11.49‰, with most values falling between +4.50‰ and +8.50‰ (Figure 4). The average $\delta^{15}N$ ($+7.47 \pm 1.53‰$, $n = 60$) is slightly higher than that of modern marine sediments (approximately +5‰, Tesdal et al., 2013). No clear stratigraphic trend is observed in $\delta^{15}N$. The $\delta^{13}C_{org}$ values are relatively stable through the study section. Most values fall in a narrow range between −34‰ and − 32‰, with an average of $-32.94 \pm 1.05‰$ ($n = 60$) (Figure 4), comparable to or slightly lower than that from the equivalent strata in the Pingquan section (Guo et al., 2013; Luo et al., 2014). TOC and TN show similar stratigraphic trends in the study section, with values ranging from 0.09% to 5.24% and 0.01% to 0.20%, respectively (Figure 4). The molar C/N ratios are generally <60 throughout the section (Figure 4), within the typical range of the Mesoproterozoic samples with low metamorphic grade (Koehler et al., 2017; Stüeken, 2013).

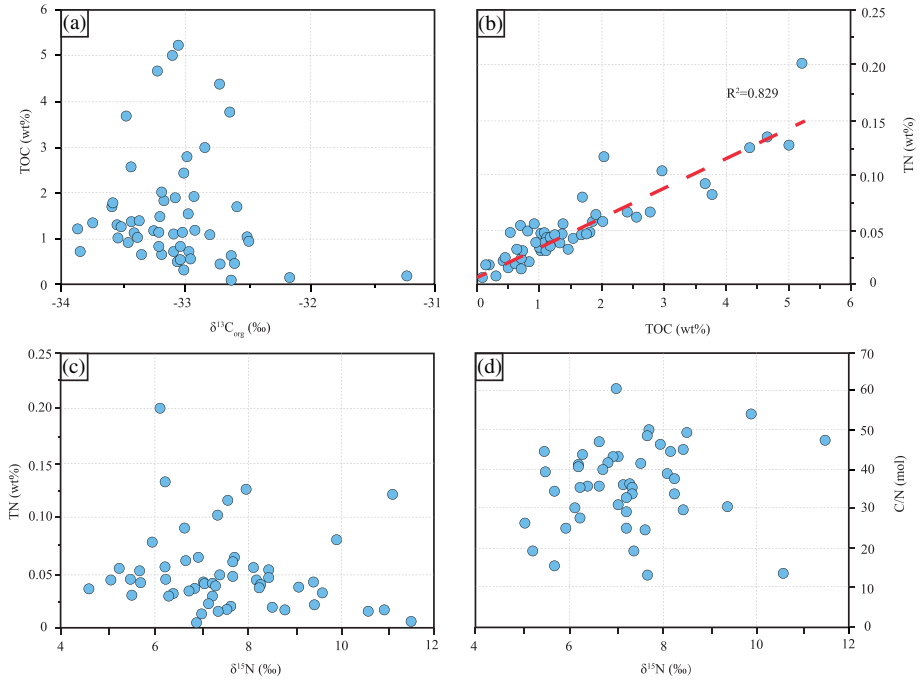

Figure 6. Cross plots of (a) TOC versus $\delta^{13}C_{org}$, (b) TOC versus TN, (c) TOC versus $\delta^{15}N$, and (d) TN versus $\delta^{15}N$.

The I/(Ca + Mg) ratios of 17 carbonate samples are dominated by low but nonzero values, ranging from 0.0 to 0.5 μmol/mol (Figure 4 and Table S2). The maximum I/(Ca + Mg) value occurs at ~133 m and reach up to 1.36 μmol/mol, but this value is still much lower than the empirically defined threshold for fully oxygenated waters (2.6 μmol/mol; Lu et al., 2010; Hardisty et al., 2017).

The major and trace element results are shown in Figure 5 and Table S3. Mo concentrations vary from 0.7 to 10.64 μg/g below 110 m, with an average of 3.4 ± 2.6 μg/g. A prominent increase in Mo content from low background values to 41.3 μg/g is observed in the interval of 130–160 m, which is followed by a decreasing trend upsection before the occurrence of high values (35.8 μg/g) near the top of the section. The concentrations of U and V show similar stratigraphic trends with that of Mo. U and V concentrations range from 0.7 to 9.9 μg/g and 10.1 to 224.2 μg/g in the first half of the study section (~30–110 m), with averages of 4.2 ± 2.1 and 99.0 ± 55.2 μg/g, respectively. Both elements show a clear increase at the interval of ca. 130–160 m. Peak values reach up to 17.2 μg/g for U and 330.2 μg/g for V before decreasing to 9.3 and 125.7 μg/g at the top of section. The stratigraphic trend observed in RSE concentrations becomes even more evident in their enrichment factors (EFs), defined as $X_{EF} = (X/Al)_S/(X/Al)_{PAAS}$ (Tribovillard et al., 2006), where X represents the concentration of concerned elements and the subscripts S and PAAS refer to sample and post-Archean Australian shale (McLennan, 2001; Taylor & McLennan, 1985). The lower part of the section shows weak to moderate enrichment for Mo (EF between 1 and 11.7) but depleted to weak enrichment for U (EF between 0.8 and 5.5) and V (EF between 0.2 and 2.3). The EFs increase to 85.6 for Mo, 13.3 for U, and 4.6 for V at ~160 m and then decrease to 20.9, 4.5 and 1.3, respectively, at the top of section (Figure 5). Similarly, P concentrations are generally low in the lower part of section (average 0.17 ± 0.08 wt%) but high at ~130–160 m (average 0.38 ± 0.29 wt%) (Figure 5).

5. Discussion

5.1. Preservation of Primary Isotopic Signals

The $\delta^{13}C_{org}$ data from the studied samples fall within the typical range of early Mesoproterozoic strata in the central North China Platform (e.g., Guo et al., 2013; Guo et al., 2015; Luo et al., 2014). Furthermore, the absence of significant correlation between $\delta^{13}C_{org}$ and TOC in our samples (Figure 6a) suggests that the degradation of organic matter during metamorphic processes had limited effect on $\delta^{13}C_{org}$, consistent

with the low metamorphic grade of these rocks (Chu et al., 2007; Li et al., 2003). Whether the bulk $\delta^{15}N$ value in sedimentary rocks can record the isotopic composition of primary seawater depends on a suite of factors, including the addition of allochthonous nitrogen, the paleogeographic setting, and diagenetic and metamorphic effects. Nitrogen in sediments is mainly present in two forms, organic-bound nitrogen and clay-bound nitrogen (mainly as NH_4^+) (see reviews in Ader et al., 2016; Stüeken et al., 2016). Clay-bound NH_4^+ is generally sourced from the *in situ* deamination of organic nitrogen, but in some cases it may have additional origins from terrestrial input and/or diagenetic fluids (e.g., Luo et al., 2018). However, the strong positive correlation between TOC and TN ($R^2 = 0.829$) in our samples, paired with a very small intercept on the TN axis (Figure 6b), indicates that the contribution of allochthonous clay-bound N, if any, was minimal. We cannot completely rule out input of detrital organic-bound N; however, this component would probably be very minor in organic-rich sediments (e.g., Jiang et al., 2010). Furthermore, it is likely that detrital organic matter would display different C/N ratios and thus manifest itself as perturbations in the TOC-versus-TN crossplot. The strong correlation between TOC and TN (Figure 6b) thus suggests that the effect of detrital organic N is insignificant in our sample set.

A recent investigation revealed that the $\delta^{15}N$ of sedimentary organic matter may show some bias compared to the sinking particles, depending on water depth and sedimentation rate (Robinson et al., 2012). Large difference can be produced at sites located off continental margins due to extended remineralization of organic matter in the water column. In contrast, on continental shelves with high sediment accumulation rates and organic matter content, sedimentary organic matter generally displays $\delta^{15}N$ values similar to that of sinking particles (Robinson et al., 2012). Since our samples reflect a relatively shallow water depth above the shelf break, the alterations of $\delta^{15}N$ during particle settling was probably minor. After sedimentation, the degradation of sedimentary organic matter during both early diagenesis and burial diagenesis releases some labile organic-bound nitrogen as NH_4^+ (e.g., Ader et al., 2016; Stüeken et al., 2016). Because this process commonly has limited isotopic fractionation, and a large proportion of the released NH_4^+ is reassimilated *in situ* by clay minerals (Müller, 1977), the isotopic effect on bulk $\delta^{15}N$ is generally negligible (Altabet et al., 1999; Freudenthal et al., 2001; Lehmann et al., 2002; Prokopenko et al., 2006; Robinson et al., 2012; Thunell et al., 2004). However, where the porewater was oxic during early diagenesis, the isotopic fractionation could reach up to 4‰ possibly due to partial oxidation of NH_4^+ in porewater (e.g., Altabet et al., 1999; Freudenthal et al., 2001; Lehmann et al., 2002; Prokopenko et al., 2006). However, the enrichment pattern of RSEs and other geochemical proxies indicates that the bottom water was suboxic to anoxic during the deposition of Member III at the study area (see discussion in section 5.3), which is inconsistent with the scenario of oxic early diagenesis.

In addition, thermal nitrogen volatilization associated with metamorphism may increase the $\delta^{15}N$ of sediment through preferential removal of ^{14}N. The associated isotopic fractionation is commonly within 1–2‰ below greenschist facies, 3–4‰ for amphibolite facies, and up to 6–10‰ for the upper amphibolite facies (e.g., Ader et al., 2016; Bebout & Fogel, 1992; Jia, 2006; Mingram & Bräuer, 2001; Stüeken et al., 2017; Thomazo & Papineau, 2013). Previous studies suggest that the metamorphic grade of the Mesoproterozoic succession in North China was below prehnite-pumpellyite facies (Chu et al., 2007; Li et al., 2003); thus, metamorphism is unlikely to have significantly altered our $\delta^{15}N$ values. Importantly, the $\delta^{15}N$ data show no obvious correlation with TN and C/N (Figures 6c and 6d), which would be the case if metamorphism had significantly perturbed our data set.

The carbonate I/(Ca + Mg) ratios are susceptible to diagenetic alteration (Hardisty et al., 2017; Lu et al., 2010; Wei et al., 2019). Laboratory experiments suggest that iodate (IO_3^-) is the only iodine species that can be incorporated into the crystal lattice of carbonate minerals (Lu et al., 2010). In most of cases, diagenetic effects that involve anoxic pore fluids would result in the reduction of carbonate-associated IO_3^- to iodide (I^-), lowering the I/(Ca + Mg) ratios of carbonates (Hardisty et al., 2017; Lu et al., 2010). The predominantly low I/(Ca + Mg) values in the study section raise the possibility of diagenetic alterations of our samples. However, they fall within the typical I/(Ca + Mg) range of the mid-Proterozoic (Hardisty et al., 2017) and show a similar stratigraphic trend to that reported from the Gan'gou section, Yanqing area (Shang et al., 2019), which is about 110 km west to the study section. We therefore conclude that our I/(Ca + Mg) results are mainly controlled by redox conditions during the time of carbonate deposition rather than by diagenetic effects.

5.2. The Origin of Positive $\delta^{15}N$ in the Gaoyuzhuang Member III

As discussed above, the $\delta^{15}N$ values of the studied samples record near-primary oceanic signals and can thus be used to reconstruct the nitrogen cycle and ocean redox state during the deposition of the Gaoyuzhuang Member III. The $\delta^{15}N$ composition of dissolved nitrogen species in seawater is controlled by the isotopic balance between input and output processes (Sigman et al., 2009; Stüeken et al., 2016). The major N source to the ocean is biological N_2 fixation, which generates N species with an isotopic composition similar to that of atmospheric N_2 (−2 to +1‰) (Zhang et al., 2014). The positive $\delta^{15}N$ values in our samples therefore indicate the preferential loss of ^{14}N during output processes. Denitrification and anammox are the two major N sinks in modern oceans (Sigman et al., 2009). Under anoxic conditions, ammonium rather than nitrate may the dominant dissolved species in seawater, and partial assimilation of ammonium into biomass could create another significant N sink. All these processes are capable of producing positive $\delta^{15}N$ values, and we will discuss each of the possibilities in detail below.

In anoxic basins, NH_4^+ may be the dominant N species and serve as the main N source to living primary producers (Higgins et al., 2012; Papineau et al., 2009; Xu et al., 2020; Yang et al., 2019). Where NH_4^+ is replete, photoautotrophs in the photic zone that preferentially uptake ^{14}N during NH_4^+ assimilation could cause an enrichment in ^{15}N in the residual NH_4^+ pool (Papineau et al., 2009; Stüeken, 2013). If this ^{15}N-enriched NH_4^+ is then transported and quantitatively assimilated by organisms elsewhere in the basin, sediments in that location could theoretically display positive $\delta^{15}N$ values. However, this scenario would be expected to create large isotopic fluctuations and spatial variability with both negative and positive $\delta^{15}N$ values distributed through the basin (Papineau et al., 2009; Stüeken, 2013). Since no negative $\delta^{15}N$ values are present in Member III of the Gaoyuzhuang Formation nor in other relevant sections in the central North China Platform, partial ammonium assimilation can probably not explain our data set.

Assuming denitrification and anammox were responsible for the removal of light ^{14}N from the ocean during the deposition of the Gaoyuzhuang Member III, two processes may be involved: partial nitrification followed by quantitative denitrification (or anammox) and partial denitrification (or anammox). We argue against the first scenario for two reasons: (1) The low but nonzero I/(Ca + Mg) values from our section (Figure 4) indicate the operation of iodide oxidation and presence of at least low levels of free oxygen in water column (Hardisty et al., 2017). Compared to iodide, ammonium is more readily oxidized to nitrite (NO_2^-) and nitrate (NO_3^-) through nitrification in the presence of free oxygen due to its lower redox potential (Lam & Kuypers, 2011). Nitrification has been documented in the presence of nanomolar levels of dissolved oxygen (e.g., Bristow et al., 2016). In the modern Black Sea, nitrification can rapidly proceed to completion under suboxic conditions near the chemocline (Fuchsman et al., 2008). (2) Partial nitrification has so far only been documented from basins with strong seasonal oxygen fluctuations (e.g., Granger et al., 2011; Morales et al., 2014) and possible in some Archean lakes with short-term oxygen oases (Thomazo et al., 2011), and in both cases the data show a very large isotopic spread. This process, however, is unlikely to have produced the consistently high $\delta^{15}N$ values in a stratigraphic succession with a thickness of ca. 150 m (Figure 4).

Denitrification and anammox preferentially release light ^{14}N to the atmosphere, rendering the residual nitrate pool in the ocean enriched in heavy ^{15}N, which, in most cases, would be quantitatively assimilated by photosynthetic organisms. These two processes are responsible for the positive $\delta^{15}N$ values in modern seawater and sediments (Sigman et al., 2009; Tesdal et al., 2013) and have been widely used to interpret positive $\delta^{15}N$ values in the geological record (Ader et al., 2014; Algeo et al., 2014; Garvin et al., 2009; Godfrey & Falkowski, 2009; Kipp et al., 2018; Koehler et al., 2017; Luo et al., 2018; Stüeken, 2013; Wang et al., 2013; Wang, Jiang, et al., 2018; Wang, Ling, et al., 2018; Zerkle et al., 2017). It is thus reasonable to infer that they also took effect during the deposition of the Gaoyuzhuang Member III. It is difficult to determine the relative contribution between denitrification and anammox since their isotopic effects are too similar (Brunner et al., 2013). In any case, the expression of the isotopic effects of partial denitrification and/or anammox requires a stable nitrate pool in the photic zone to avoid quantitative reduction. Our data are thus evidence for an oxic upper ocean, though deep oceans may have been dominated by anoxic conditions (see details in section 5.3).

5.3. Ocean Redox Evolution During the Deposition of the Gaoyuzhuang Member III

Considering the occurrence of diverse eukaryotic fossils in the Gaoyuzhuang Member III (Shi et al., 2017; Zhu et al., 2016), environmental reconstructions of this critical period have become a topic of wide

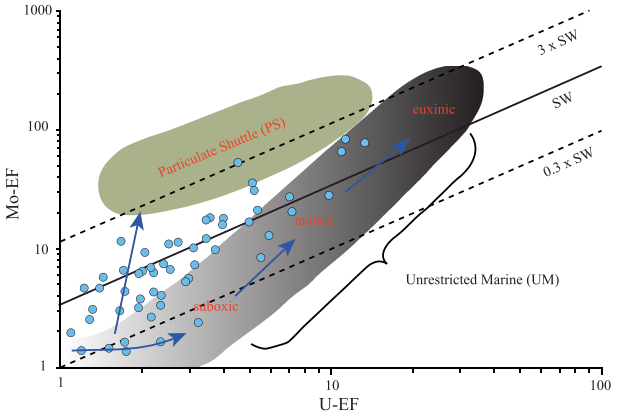

Figure 7. Mo-EF versus U-EF of Member III in the Xinlong section (background figure modified from Algeo and Tribovillard (2009)). Note that the thresholds distinguishing suboxic, anoxic, and euxinic conditions suggested by Algeo and Tribovillard (2009) could be lower during the Precambrian relative to the Phanerozoic due to the low seawater Mo and U pools (Sahoo et al., 2012).

interest. Previous systematic carbon isotope studies from the Pingquan section, about 100 km to the northeast from our study site, reveal relatively low $\delta^{13}C_{org}$ values for most of the Gaoyuzhuang Member III, which were interpreted as admixture of primary and secondary (chemoautotrophic and/or anaerobic photoautotrophic) production due to the presence of a shallow chemocline (Guo et al., 2013; Luo et al., 2014). Sulfur isotope studies from the same interval also suggested a small sulfate pool related to low oxygen levels in the atmosphere-ocean system at that time (Guo et al., 2015; Luo et al., 2015). Recently, Zhang et al. (2018) reported persistently negative Ce anomalies in REE patterns in the Gaoyuzhuang Member III in the Jixian section, which, along with a prominent negative carbonate $\delta^{13}C$ excursion, was interpreted as evidence for a significant oxygenation event. This inference is further consolidated by the elevated I/(Ca + Mg) values from the same interval in the Gan'gou section, Yanqing area (Shang et al., 2019). Further semiquantitative estimates indicate that oxygen may have increased up to ≥4% PAL before shifting back to low background values after the oxygenation event (Shang et al., 2019).

To further elucidate local redox conditions, we combined RSEs, Mo-U covariation, I/(Ca + Mg), and $\delta^{13}C_{org}$. In the lower part of Member III (~50–120 m) (Figure 5), the RSEs (Mo, U, and V) show little to moderate enrichment, which cannot be explicitly attributed to any specific redox condition, especially during the Precambrian (Sahoo et al., 2012). For comparison, the upper part of the study interval (~130–200 m) is characterized by moderate to strong enrichments of Mo, U, and V, indicative of a locally anoxic and/or euxinic environments (Scott & Lyons, 2012; Tribovillard et al., 2006). The increase of RSEs contents may reflect an expanded dissolved reservoir in response to the inferred short-lived oxygenation event (Shang et al., 2019). The Mo-U covariation can provide further insight into local redox conditions (Algeo & Tribovillard, 2009; Tribovillard et al., 2012). In suboxic environments, the enrichment of U is generally larger than that of Mo because the soluble U(VI) ion is readily reduced to insoluble U(IV) under these conditions. As benthic environments become more reducing and sulfidic, uptake of authigenic Mo will eventually exceed authigenic U, resulting in elevated Mo_{au}/U_{au} (where "au" stands for authigenic), unless strong basin restriction resulted in depletion of seawater Mo levels (Algeo & Tribovillard, 2009; Tribovillard et al., 2012). With the exception of a few data points, most of our samples show moderate to high enrichment of Mo relative to U (Figure 7), suggesting predominately suboxic to anoxic bottom water conditions at the site of deposition, paired with a connection to a relatively large oxic Mo reservoir. However, very few of our Mo data approach Phanerozoic enrichments, suggesting that either (a) Mo drawdown was nonquantitative because dissolved sulfide levels were locally too low or (b) perhaps more likely the marine Mo reservoir was not as extensive as today and the ocean therefore not widely oxygenated, consistent with previous interpretations (Reinhard et al., 2013; Sahoo et al., 2012; Scott et al., 2008). Supporting evidence can also be found in the I/(Ca + Mg) profile in our section. Almost all I/(Ca + Mg) values are dominated by extremely low values (<0.5 μmol/mol) (Figure 4), indicating oxygen-depleted conditions (Hardisty et al., 2017; Lu et al., 2010; Shang et al., 2019). Nevertheless, the inferred short-lived oxygenation event (Shang et al., 2019) may be captured by one sample at ~133 m (Figure 4), but the I/(Ca + Mg) value (1.36 μmol/mol) does not reach as high as those observed in the Gan'gou section (Shang et al., 2019) and is still much lower than the oxic threshold (2.6 μmol/mol; Lu et al., 2010; Hardisty et al., 2017; Shang et al., 2019), suggesting that the study section may be located close to the chemocline. Additionally, $\delta^{13}C_{org}$ values in our study section are overall comparable to or slightly lower than those reported from the equivalent interval in the Pingquan section, possibly associated with an elevated contribution from secondary production in an anoxic environment (Guo et al., 2013; Luo et al., 2014).

In summary, integrated geochemical proxies suggest that the Gaoyuzhuang Member III at our study site was deposited in a largely suboxic-anoxic environment, possibly close to or below the chemocline. The new data coupled with previous ones from other correlative sections reveal that the ocean in North China was still strongly redox stratified, but a pulse of ocean oxygenation (Shang et al., 2019; Zhang et al., 2018) may have resulted in the deepening of chemocline.

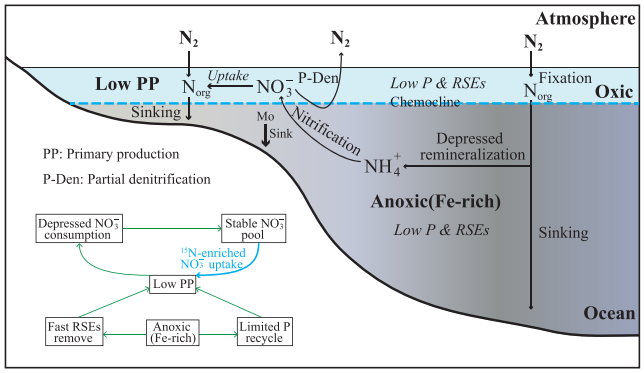

Figure 8. Schematic diagram showing the N cycle in a strongly stratified ocean during the deposition of the Gaoyuzhuang Formation. Inset indicates feedbacks between ocean redox, macronutrients, RSEs, and primary productivity. During the deposition of the Gaoyuzhuang Member III, prevailing anoxic and Fe-rich conditions through the basin probably resulted in substantial sequestration of P and RSEs and depressed organic P recycling. Low P and RSEs limited primary productivity, which would significantly reduce the consumption of nitrate and maintained a fairly stable NO_3^- reservoir at least in the oxic layer of the surface ocean. Assimilation of ^{15}N-enriched NO_3^- would have produced organic matter with positive $\delta^{15}N$ that was subsequently deposited in sediments.

5.4. Preservation of an Aerobic Nitrogen Cycle Signal in a Redox-Stratified Ocean

Models suggest that in a largely anoxic ocean such as during most time of the Proterozoic (see review in Lyons et al., 2014), fixed nitrogen (particularly NO_3^-) would be scarce due to high rates of conversion to N_2 by denitrification and anammox (Fennel et al., 2005). Consequently, only a small fraction of ecosystems could have been sustained by nitrate as the major nitrogen source; most organisms probably relied on N_2-fixation and the direct product ammonium. The isotopic effects of denitrification would thus have been undetectable (Kipp et al., 2018). Such a situation has been documented from some modern and ancient stratified basins. For instance, in the modern Black Sea, the largest anoxic basin with a chemocline at depth of ~90 m, consumption of NO_3^- by denitrification is near quantitative; thus, the nitrate concentration in the oxic surface layer of the Black Sea (<3.5 μM; Fuchsman et al., 2008) is almost tenfold lower than that of the open oceans (~30 μM; Lam & Kuypers, 2011), leaving N_2 fixation as the dominated pathway fueling primary productivity. Sedimentary $\delta^{15}N$ values are thus close to that of atmospheric N_2 (Fulton et al., 2012). Even in the semirestricted Cariaco Basin, the second largest modern anoxic marine system with a much deeper chemocline (at depth of ~280 m), water column denitrification has only minor effects on the net isotopic composition of sediments due to near-quantitative nitrate consumption at the chemocline, leading to the residual and sediment $\delta^{15}N$ moderately lower than that of open oceans (but higher than that of the Black Sea) (Thunell et al., 2004). Similarly, during the Cretaceous OAE 2 (Ocean Anoxic Event 2) when anoxic water impinged on the photic zone, nitrate was possibly depleted in the surface ocean. As a consequence, primary productivity appears to have been mainly driven by N_2 fixation and/or NH_4^+ assimilation, as evidenced by predominately low $\delta^{15}N$ values documented in many sections across the Tethys ocean and proto-Atlantic region (Higgins et al., 2012; Jenkyns et al., 2007; Junium & Arthur, 2013).

In light of these observations, the positive $\delta^{15}N$ values from the Gaoyuzhuang Member III in our studied section, which we interpret as partial denitrification and subsequently quantitative assimilation of ^{15}N-enriched residual nitrate, are counterintuitive because our RSEs and iodine data indicate that the ocean was strongly stratified during this period (see section 5.3). Importantly, the depth of the chemocline during the most of time of the Gaoyuzhuang Member III may be quite shallow, possibly even reaching up to intertidal zone at certain time periods (Luo et al., 2014). We therefore speculate that denitrification was rate limited. Generally, the rate of denitrification is dependent on the extent of anoxia and the availability of organic matter, the latter of which is directly related to primary productivity. To allow for the preservation of the signal of nitrate assimilation in a strongly stratified ocean, the effect of expanded anoxia on denitrification has to be offset by decreased primary productivity (Figure 8). Indeed, the mid-Proterozoic was likely a period of low primary productivity due to scarcity of important macronutrients and micronutrients and trace elements in largely anoxic oceans (Anbar & Knoll, 2002; Kipp et al., 2018; Reinhard et al., 2017, 2020; Scott et al., 2008). In support of this inference, a recent triple oxygen isotope study from sedimentary sulfates suggests limited mid-Proterozoic primary productivity (Crockford et al., 2018). Further, modeling calculations also indicate that primary productivity in the mid-Proterozoic ocean may have been one to two orders lower than today (Laakso & Schrag, 2019; Ozaki et al., 2019). The decline of primary productivity would have been conducive to maintaining a fairly stable NO_3^- pool at least in the surface oxic layer of the mid-Proterozoic ocean, consistent with the high $\delta^{15}N$ values from the Gaoyuzhuang Member III (Figure 8). This model can also be used to explain the positive $\delta^{15}N$ values documented in the onshore areas of other Mesoproterozoic basins (Koehler et al., 2017; Stüeken, 2013). An important implication of this interpretation is that local anoxia was not driven by high rates of productivity as in modern oxygen minimum zones, but instead, it was probably driven by influx of anoxic deep waters into this basin. If so, then the moderate enrichments in RSEs were probably not caused by local drawdown from a large marine reservoir but instead

by trapping of fluvial Mo in anoxic nearshore settings as described from the late Mesoproterozoic Taoudeni basin (Gilleaudeau & Kah, 2013).

5.5. Implication for Early Eukaryote Evolution

Though the mid-Proterozoic has long been considered as a period of evolutionary stasis in light of much lower abundance and diversity of eukaryotes compared to the Neoproterozoic (e.g., Knoll, 2014), recent paleontological studies indicated an evolutionary leap of eukaryotes at the onset of the Mesoproterozoic (Shi et al., 2017; Zhu et al., 2016). Shi et al. (2017) reported a number of putative eukaryotic microfossils from the Gaoyuzhuang Member III at Jixian, Tianjin, North China. Importantly, decimeter-scale multicellular eukaryotes with unknown phylogenetic affinity have been discovered from the same interval in the Qianxi and Kuancheng areas (Zhu et al., 2016). The availability of fixed nitrogen in the ocean, in particular nitrate, should have been important for the rise of eukaryotes, because they are unable to fix N_2 themselves and they are easily outcompeted for ammonium by prokaryotes (Anbar & Knoll, 2002; Koehler et al., 2017). However, the linkage between the early Mesoproterozoic appearance of complex eukaryotes and the marine nitrogen cycle has so far remained elusive.

The persistently elevated $\delta^{15}N$ values from our study indicate the existence of a fairly stable NO_3^- pool at least in the surface oxic layer during the deposition of the Gaoyuzhuang Member III. As in the modern ocean (Karl et al., 2001), this NO_3^- could have fueled eukaryotic primary producers. Indeed, the bioavailability of nitrate in the Paleoproterozoic surface ocean has previously been suggested to have facilitated the emergence and initial development of eukaryotic life (e.g., Kipp et al., 2018; Zerkle et al., 2017), and even the rapid diversification of metazoans has been linked to an increase of the NO_3^- pool in the late Neoproteroozic and early Cambrian (Wang, Jiang, et al., 2018; Wang, Ling, et al., 2018). Thus, our $\delta^{15}N$ data presented here may reinforce the connection between nutrient N cycling and eukaryotic evolution in early Mesoproterozoic ocean.

A notable observation, however, is that the occurrence of most eukaryotic fossils was restricted to the middle part of the Gaoyuzhuang Member III despite the persistently high $\delta^{15}N$ throughout this unit (Figure 4). The simplest explanation for this phenomenon could be taphonomic bias. Alternatively, other factors beyond nitrate availability may have contributed to regulating eukaryotic development. Indeed, in the middle part of Member III where most eukaryotic fossils were discovered (Shi et al., 2017; Zhu et al., 2016), the enrichments of some RSEs (e.g., Mo, V, and U) show an apparent increase from low background values (Figure 5), possibly indicative of an increased RSEs pool in seawater in response to the expansion of oxic environments (e.g., Sahoo et al., 2012; Scott et al., 2008). Elevated I/(Ca + Mg) values coupled with a 3.5‰ negative shift in both $\delta^{13}C_{carb}$ and $\delta^{13}C_{org}$ have also been observed in this interval, providing further evidence of a pulsed rise of O_2 levels (Shang et al., 2019). Phosphorus concentration also shows a marked increase in the same interval (Figure 5), possibly associated with a short-lived elevation of oceanic P levels due to a shrinkage in the anoxic sink (e.g., Reinhard et al., 2017). Thus, the concurrence of these biological and geochemical signals suggests that the circa 1.56 Ga evolutionary leap was not driven by nitrate availability alone but instead the result of complex feedbacks between ocean redox, primary productivity, and the cycling of multiple bio-essential elements, including N, P, and possibly trace metals.

6. Conclusions

Integrated studies of $\delta^{15}N$, $\delta^{13}C_{org}$, and major and trace element contents were conducted on Member III of the Mesoproterozoic Gaoyuzhuang Formation (ca. 1.60–1.54 Ga) in the North China Craton, from which decimeter-scale eukaryotic fossils were recently reported. Several lines of evidence suggest that the Gaoyuzhuang Member III in the studied section was deposited in a largely suboxic to anoxic environment as evidenced by RSEs enrichments (e.g., Mo, U, and V), Mo-U covariation, depleted $\delta^{13}C_{org}$, and very low I/(Ca + Mg). These data, coupled with previous results from other correlative sections, imply that the Mesoproterozoic ocean in North China was redox stratified, despite potential pulses of ocean oxygenation and fluctuations of the chemocline. This redox structure provides a framework for the interpretation of the $\delta^{15}N$ data. The stable and high $\delta^{15}N$ values from the study section are best interpreted as the result of partial denitrification, which preferentially removed ^{14}N from seawater, implying the presence of a fairly stable nitrate pool at least in the oxic surface waters. The operation of an aerobic N cycle in a strongly

stratified ocean, although rarely seen in modern oceans, could be attributed to the combined effects of expanded oxic surface waters and low primary productivity such that denitrification was nonquantitative. The increased availability of nitrate may have contributed to providing a habitable environment for eukaryotic organisms. However, the lack of eukaryotic fossils in large parts of the section, despite elevated $\delta^{15}N$ values, suggests that besides nitrate availability also micronutrients and P concentrations played an important role in this evolutionary leap at circa 1.56 Ga. The rise of eukaryotes was evidently a result of complex feedbacks between ocean redox, primary productivity, and bio-essential element cycles.

Acknowledgments
The research is funded by National Natural Science Foundation of China (41930320 and 41872032) and the Fundamental Research Funds for the Central Universities (2652017228). Thanks are given to Haoming Wei, Jianbai Ma, Zhan Zhao, and Hao Fang for their assistance in field work and Lianjun Feng for his help in organic carbon isotope analysis. This paper is greatly improved by valuable comments from Noah Planavsky and one anonymous reviewer. All data present in this paper are provided in the supporting information and are available online (https://zenodo.org/record/3701935#.XnEaPCIUDL9).

References

Ader, M., Sansjofre, P., Halverson, G. P., Busigny, V., Trindade, R. I., Kunzmann, M., & Nogueira, A. C. (2014). Ocean redox structure across the late Neoproterozoic oxygenation event: A nitrogen isotope perspective. *Earth and Planetary Science Letters*, *396*(1), 1–13. http://doi.org/10.1016/j.epsl.2014.03.042

Ader, M., Thomazo, C., Sansjofre, P., Busigny, V., Papineau, D., Laffont, R., et al. (2016). Interpretation of the nitrogen isotopic composition of Precambrian sedimentary rocks: Assumptions and perspectives. *Chemical Geology*, *429*(46), 93–110. http://doi.org/10.1016/j.chemgeo.2016.02.010

Algeo, T. J., Meyers, P. A., Robinson, R. S., Rowe, H., & Jiang, G. Q. (2014). Icehouse-greenhouse variations in marine denitrification. *Biogeosciences*, *11*(4), 14769–14813. https://doi.org/10.5194/bg-11-1273-2014

Algeo, T. J., & Tribovillard, N. (2009). Environmental analysis of paleoceanographic systems based on molybdenum–uranium covariation. *Chemical Geology*, *268*(3–4), 211–225. http://doi.org/10.1016/j.chemgeo.2009.09.001

Altabet, M. A., Pilskaln, C., Thunell, R., Pride, C., Sigman, D., Chavez, F., & Francois, R. (1999). The nitrogen isotope biogeochemistry of sinking particles from the margin of the eastern north pacific. *Deep Sea Research Part I Oceanographic Research Papers*, *46*(4), 655–679. http://doi.org/10.1016/S0967-0637(98)00084-3

Anbar, A. D., & Knoll, A. H. (2002). Proterozoic ocean chemistry and evolution: A bioinorganic bridge? *Science*, *297*(5584), 1137–1142. http://doi.org/10.1126/science.1069651

Bebout, G. E., & Fogel, M. L. (1992). Nitrogen-isotope compositions of metasedimentary rocks in the Catalina Schist, California: Implications for metamorphic devolatilization history. *Geochimica et Cosmochimica Acta*, *56*(7), 2839–2849. https://doi.org/10.1016/0016-7037(92)90363-N

Bristow, L. A., Dalsgaard, T., Tiano, L., Mills, D. B., Bertagnolli, A. D., Wright, J. J., et al. (2016). Ammonium and nitrite oxidation at nanomolar oxygen concentrations in oxygen minimum zone waters. *Proceedings of the National Academy of Sciences*, *113*(38), 10601–10606. http://doi.org/10.1073/pnas.1600359113

Brunner, B., Contreras, S., Lehmann, M. F., Matantseva, O., Rollog, M., Kalvelage, T., et al. (2013). Nitrogen isotope effects induced by anammox bacteria. *Proceedings of the National Academy of Sciences*, *110*(47), 18994–18999. http://doi.org/10.1073/pnas.1310488110

Canfield, D. E., Zhang, S., Frank, A. B., Wang, X., Wang, H., Su, J., et al. (2018). Highly fractionated chromium isotopes in Mesoproterozoic-aged shales and atmospheric oxygen. *Nature Communications*, *9*(1), 2871. http://doi.org/10.1038/s41467-018-05263-9

Chu, X. L., Zhang, T. G., Zhang, Q. R., & Lyons, T. W. (2007). Sulfur and carbon isotope records from 1700 to 800 Ma carbonates of the Jixian section, Northern China: implications for secular isotope variations in Proterozoic seawater and relationships to global supercontinental events. *Geochimica et Cosmochimica Acta*, *71*(19), 4668–4692. http://doi.org/10.1016/j.gca.2007.07.017

Cole, D. B., Reinhard, C. T., Wang, X., Gueguen, B., Halverson, G. P., Gibson, T., et al. (2016). A shale-hosted Cr isotope record of low atmospheric oxygen during the Proterozoic. *Geology*, *44*(7), 555–558. http://doi.org/10.1130/g37787.1

Crockford, P. W., Hayles, J. A., Bao, H., Planavsky, N. J., Bekker, A., Fralick, P. W., et al. (2018). Triple oxygen isotope evidence for limited mid-Proterozoic primary productivity. *Nature*, *559*(7715), 613–616. http://doi.org/10.1038/s41586-018-0349-y

Derry, L. A. (2015). Causes and consequences of mid-Proterozoic anoxia. Geophysical. *Research Letters*, *42*. 2015GL065333

Fennel, K., Follows, M., & Falkowski, P. G. (2005). The co-evolution of the nitrogen, carbon and oxygen cycles in the Proterozoic ocean. *American Journal of Science*, *305*(6–8), 526–545. http://doi.org/10.2475/ajs.305.6-8.526

Freudenthal, T., Wagner, T., Wenzhöfer, F., Zabel, M., & Wefer, G. (2001). Early diagenesis of organic matter from sediments of the eastern subtropical Atlantic: evidence from stable nitrogen and carbon isotopes. *Geochimica et Cosmochimica Acta*, *65*(11), 1795–1808. http://doi.org/10.1016/S0016-7037(01)00554-3

Fuchsman, C. A., Murray, J. W., & Konovalov, S. K. (2008). Concentration and natural stable isotope profiles of nitrogen species in the Black Sea. *Marine Chemistry*, *111*(1), 90–105. http://doi.org/10.1016/j.marchem.2008.04.009

Fulton, J. M., Arthur, M. A., & Freeman, K. H. (2012). Black sea nitrogen cycling and the preservation of phytoplankton $\delta^{15}N$ signals during the Holocene. *Global Biogeochemical Cycles*, *26*, GB2030. http://doi.org/10.1029/2011gb004196

Gao, L. Z., Zhang, C. H., Yin, C. Y., Shi, X. Y., Wang, Z. Q., Liu, Y. M., et al. (2008). SHRIMP zircon ages: Basis for refining the chronostratigraphic classification of the Meso- and Neoproterozoic strata in North China old land. *Acta Geosci. Sin.*, *29*, 366–376. (in Chinese with English abstract)

Garvin, J., Buick, R., Anbar, A. D., Arnold, G. L., & Kaufman, A. J. (2009). Isotopic evidence for an aerobic nitrogen cycle in the latest Archean. *Science*, *323*(5917), 1045–1048. http://doi.org/10.1126/science.1165675

Gilleaudeau, G. J., & Kah, L. C. (2013). Oceanic molybdenum drawdown by epeiric sea expansion in the Mesoproterozoic. *Chemical Geology*, *356*, 21–37. http://doi.org/10.1016/j.chemgeo.2013.07.004

Gilleaudeau, G. J., & Kah, L. C. (2015). Heterogeneous redox conditions and a shallow chemocline in the Mesoproterozoic ocean: Evidence from carbon–sulfur–iron relationships. *Precambrian Research*, *257*, 94–108. http://doi.org/10.1016/j.precamres.2014.11.030

Godfrey, L. V., & Falkowski, P. G. (2009). The cycling and redox state of nitrogen in the Archaean ocean. *Nature Geoscience*, *2*(10), 725–729. http://doi.org/10.1038/ngeo633

Granger, J., Prokopenko, M. G., Sigman, D. M., Mordy, C. W., Morse, Z. M., Morales, L. V., et al. (2011). Coupled nitrification-denitrification in sediment of the eastern Bering Sea shelf leads to ^{15}N enrichment of fixed n in shelf waters. *Journal of Geophysical Research*, *116*, C11006. http://doi.org/10.1029/2010jc006751

Guo, H., Du, Y., Kah, L. C., Hu, C., Huang, J., Huang, H., et al. (2015). Sulfur isotope composition of carbonate-associated sulfate from the Mesoproterozoic Jixian Group, North China: Implications for the marine sulfur cycle. *Precambrian Research*, *266*, 319–336. https://doi.org/10.1016/j.precamres.2015.05.032

Guo, H., Du, Y., Kah, L. C., Huang, J., Hu, C., Huang, H., & Yu, W. (2013). Isotopic composition of organic and inorganic carbon from the Mesoproterozoic Jixian Group, North China: Implications for biological and oceanic evolution. *Precambrian Research*, *224*(1), 169–183. http://doi.org/10.1016/j.precamres.2012.09.023

Hardisty, D. S., Lu, Z., Bekker, A., Diamond, C. W., Gill, B. C., Jiang, G., et al. (2017). Perspectives on Proterozoic surface ocean redox from iodine contents in ancient and recent carbonate. *Earth and Planetary Science Letters*, *463*, 159–170. https://doi.org/10.1016/j.epsl.2017.01.032

Higgins, M. B., Robinson, R. S., Husson, J. M., Carter, S. J., & Pearson, A. (2012). Dominant eukaryotic export production during ocean anoxic events reflects the importance of recycled NH_4^+. *Proceedings of the National Academy of Sciences*, *109*(7), 2269–2274. http://doi.org/10.1073/pnas.1104313109

Javaux, E. J., & Lepot, K. (2018). The Paleoproterozoic fossil record: Implications for the evolution of the biosphere during Earth's middle-age. *Earth-Science Reviews*, *176*, 68–86. https://doi.org/10.1016/j.earscirev.2017.10.001

Jenkyns, H. C., Matthews, A., Tsikos, H., & Erel, Y. (2007). Nitrate reduction, sulfate reduction, and sedimentary iron isotope evolution during the Cenomanian-Turonian oceanic anoxic event. *Paleoceanography*, *22*(3), PA3208. http://doi.org/10.1029/2006pa001355

Jia, Y. (2006). Nitrogen isotope fractionations during progressive metamorphism: A case study from the Paleozoic Cooma metasedimentary complex, southeastern Australia. *Geochimica et Cosmochimica Acta*, *70*(20), 5201–5214. https://doi.org/10.1016/j.gca.2006.08.004

Jiang, G., Wang, X., Shi, X., Zhang, S., Xiao, S., & Dong, J. (2010). Organic carbon isotope constraints on the dissolved organic carbon (DOC) reservoir at the Cryogenian-Ediacaran transition. *Earth and Planetary Science Letters*, *299*(1), 159–168. https://doi.org/10.1016/j.epsl.2010.08.031

Junium, C. K., & Arthur, M. A. (2013). Nitrogen cycling during the Cretaceous, Cenomanian-Turonian oceanic anoxic event II. *Geochemistry Geophysics Geosystems*, *8*, Q03002. http://doi.org/10.1029/2006gc001328

Karl, D. M., Bidigare, R. R., & Letelier, R. M. (2001). Long-term changes in plankton community structure and productivity in the North Pacific Subtropical Gyre: The domain shift hypothesis. *Deep Sea Research Part II Topical Studies in Oceanography*, *48*(8), 1449–1470. https://doi.org/10.1016/S0967-0645(00)00149-1

Kipp, M. A., Stüeken, E. E., Misuk, Y., Andrey, B., & Roger, B. (2018). Pervasive aerobic nitrogen cycling in the surface ocean across the Paleoproterozoic Era. *Earth and Planetary Science Letters*, *500*, 117–126. https://doi.org/10.1016/j.epsl.2018.08.007

Knoll, A. H. (2014). Paleobiological perspectives on early eukaryotic evolution. *Cold Spring Harbor Perspectives in Biology*, *6*(1), 1–14. http://doi.org/10.1101/cshperspect.a016121

Koehler, M. C., Stüeken, E. E., Kipp, M. A., Buick, R., & Knoll, A. H. (2017). Spatial and temporal trends in Precambrian nitrogen cycling: A Mesoproterozoic offshore nitrate minimum. *Geochimica et Cosmochimica Acta*, *198*, 315–337. https://doi.org/10.1016/j.gca.2016.10.050

Laakso, T. A., & Schrag, D. P. (2019). A small marine biosphere in the Proterozoic. *Geobiology*, *17*(2), 161–171. http://doi.org/10.1111/gbi.12323

Lam, P., & Kuypers, M. M. (2011). Microbial nitrogen cycling processes in oxygen minimum zones. *Annual Review of Marine Science*, *3*(1), 317–345. http://doi.org/10.1146/annurev-marine-120709-142814

Lehmann, M. F., Bernasconi, S. M., Barbieri, A., & Mckenzie, J. A. (2002). Preservation of organic matter and alteration of its carbon and nitrogen isotope composition during simulated and in situ early sedimentary diagenesis. *Geochimica et Cosmochimica Acta*, *66*(20), 3573–3584. http://doi.org/10.1016/S0016-7037(02)00968-7

Li, C., Peng, P., Sheng, G., Fu, J., & Yan, Y. (2003). A molecular and isotopic geochemical study of Meso- to Neoproterozoic (1.73–0.85 Ga) sediments from the Jixian section, Yanshan Basin, North China. *Precambrian Research*, *125*(3–4), 337–356. http://doi.org/10.1016/S0301-9268(03)00111-6

Li, C., Planavsky, N. J., Love, G. D., Reinhard, C. T., Hardisty, D., Feng, L., et al. (2015). Marine redox conditions in the middle Proterozoic ocean and isotopic constraints on authigenic carbonate formation: Insights from the Chuanlinggou Formation, Yanshan Basin, North China. *Geochimica et Cosmochimica Acta*, *150*, 90–105. http://doi.org/10.1016/j.gca.2014.12.005

Li, H. K., Zhu, S. X., Xiang, Z. Q., Su, W. B., Lu, S. N., Zhou, H. Y., et al. (2010). Zircon U-Pb datingon tuff bed from Gaoyuzhuang Formation in Yanqing, Beijing: Further constraints on the new subdivision of the Mesoproterozoic stratigraphy in the northern North China Craton. *Acta Petrologica Sinica*, *26*(7), 2131–2140.

Liu, X. M., Kah, L. C., Knoll, A. H., Cui, H., Kaufman, A. J., Shahar, A., & Hazen, R. M. (2016). Tracing Earth's O_2 evolution using Zn/Fe ratios in marine carbonates. *Geochemical Perspectives Letters*, *2*(1), 24–34. http://doi.org/10.7185/geochemlet.1603

Lu, S., Zhao, G., Wang, H., & Hao, G. (2008). Precambrian metamorphic basement and sedimentary cover of the North China Craton: A review. *Precambrian Research*, *160*(1), 77–93. https://doi.org/10.1016/j.precamres.2007.04.017

Lu, S. N., & Li, H. M. (1991). A precise U-Pb single zircon age determination for the volcanics of the Dahongyu Formation Changcheng System in Jixian. *Bull. Chin. Acad. Geol. Sci.*, *22*, 137–146. (in Chinese with English abstract)

Lu, Z., Jenkyns, H. C., & Rickaby, R. E. M. (2010). Iodine to calcium ratios in marine carbonate as a paleo-redox proxy during oceanic anoxic events. *Geology*, *38*(12), 1107–1110. http://doi.org/10.1130/g31145.1

Luo, G., Junium, C. K., Izon, G., Ono, S., Beukes, N. J., Algeo, T. J., et al. (2018). Nitrogen fixation sustained productivity in the wake of the Palaeoproterozoic Great Oxygenation Event. *Nature Communications*, *9*(1), 978. http://doi.org/10.1038/s41467-018-03361-2

Luo, G., Junium, C. K., Kump, L. R., Huang, J., Li, C., Feng, Q., et al. (2014). Shallow stratification prevailed for ~1700 to ~1300 Ma ocean: Evidence from organic carbon isotopes in the North China Craton. *Earth and Planetary Science Letters*, *400*, 219–232. http://doi.org/10.1016/j.epsl.2014.05.020

Luo, G., Ono, S., Huang, J., Algeo, T. J., Li, C., Zhou, L., et al. (2015). Decline in oceanic sulfate levels during the early Mesoproterozoic. *Precambrian Research*, *258*, 36–47. http://doi.org/10.1016/j.precamres.2014.12.014

Lyons, T. W., Reinhard, C. T., & Planavsky, N. J. (2014). The rise of oxygen in Earth's early ocean and atmosphere. *Nature*, *506*(7488), 307–315. http://doi.org/10.1038/nature13068

McLennan, S. M. (2001). Relationships between the trace element composition of sedimentary rocks and upper continental crust. *Geochemistry, Geophysics, Geosystems*, *2*(4), 1021. http://doi.org/10.1029/2000gc000109

Mei, M. (2005). Preliminary study on sequence-stratigraphic position and origin for Molar-tooth structure of the Gaoyuzhuang Formation of Mesoproterozoic at Jixian section in Tianjin. *Journal of Palaeogeography*, *7*, 437–447. (in Chinese with English abstract)

Miao, L., Moczydłowska, M., Zhu, S., & Zhu, M. (2019). New record of organic-walled, morphologically distinct microfossils from the late Paleoproterozoic Changcheng Group in the Yanshan Range, North China. *Precambrian Research*, *321*, 172–198. https://doi.org/10.1016/j.precamres.2018.11.019

Mingram, B., & Bräuer, K. (2001). Ammonium concentration and nitrogen isotope composition in metasedimentary rocks from different tectonometamorphic units of the European Variscan Belt. *Geochimica et Cosmochimica Acta*, *65*(2), 273–287. https://doi.org/10.1016/S0016-7037(00)00517-2

Morales, L. V., Granger, J., Chang, B. X., Prokopenko, M. G., Plessen, B., Gradinger, R., & Sigman, D. M. (2014). Elevated $^{15}N/^{14}N$ in particulate organic matter, zooplankton, and diatom frustule-bound nitrogen in the ice-covered water column of the Bering Sea eastern shelf. *Deep Sea Research Part II: Topical Studies in Oceanography*, *109*, 100–111. https://doi.org/10.1016/j.dsr2.2014.05.008

Müller, P. J. (1977). CN ratios in Pacific deep-sea sediments: Effect of inorganic ammonium and organic nitrogen compounds sorbed by clays. *Geochimica et Cosmochimica Acta*, *41*(6), 765–776. https://doi.org/10.1016/0016-7037(77)90047-3

Ozaki, K., Reinhard, C. T., & Tajika, E. (2019). A sluggish mid-Proterozoic biosphere and its effect on Earth's redox balance. *Geobiology*, *17*(1), 3–11. http://doi.org/10.1111/gbi.12317

Papineau, D., Purohit, R., Goldberg, T., Pi, D., Shields, G. A., Bhu, H., et al. (2009). High primary productivity and nitrogen cycling after the Paleoproterozoic phosphogenic event in the Aravalli Supergroup, India. *Precambrian Research*, *171*(1–4), 37–56. http://doi.org/10.1016/j.precamres.2009.03.005

Partin, C. A., Bekker, A., Planavsky, N. J., Scott, C. T., Gill, B. C., Li, C., et al. (2013). Large-scale fluctuations in Precambrian atmospheric and oceanic oxygen levels from the record of U in shales. *Earth and Planetary Science Letters*, *369–370*, 284–293. http://doi.org/10.1016/j.epsl.2013.03.031

Planavsky, N. J., Cole, D. B., Reinhard, C. T., Diamond, C., Love, G. D., Luo, G., et al. (2016). No evidence for high atmospheric oxygen levels 1,400 million years ago. *Proceedings of the National Academy of Sciences*, *113*(19), E2550. http://doi.org/10.1073/pnas.1601925113

Planavsky, N. J., McGoldrick, P., Scott, C. T., Li, C., Reinhard, C. T., Kelly, A. E., et al. (2011). Widespread iron-rich conditions in the mid-Proterozoic ocean. *Nature*, *477*(7365), 448–451. http://doi.org/10.1038/nature10327

Planavsky, N. J., Reinhard, C. T., Wang, X., Thomson, D., McGoldrick, P., Rainbird, R. H., et al. (2014). Low Mid-Proterozoic atmospheric oxygen levels and the delayed rise of animals. *Science*, *346*(6209), 635–638. http://doi.org/10.1126/science.1258410

Poulton, S. W., & Canfield, D. E. (2011). Ferruginous conditions: A dominant feature of the ocean through Earth's history. *Elements*, *7*(2), 107–112. http://doi.org/10.2113/gselements.7.2.107

Prokopenko, M. G., Hammond, D. E., Berelson, W. M., Bernhard, J. M., Stott, L., & Douglas, R. (2006). Nitrogen cycling in the sediments of Santa Barbara basin and Eastern Subtropical North Pacific: Nitrogen isotopes, diagenesis and possible chemosymbiosis between two lithotrophs (Thioploca and Anammox)—"riding on a glider". *Earth and Planetary Science Letters*, *242*(1–2), 186–204. http://doi.org/10.1016/j.epsl.2005.11.044

Qiao, X. F., & Gao, L. Z. (2007). Mesoproterozoic palaeoearthquake and palaeogeogra-phy in Yan-Liao Aulacogen. *J. Palaeogeogr.*, *9*, 337–352. (in Chinese with English abstract)

Qiao, X. F., Gao, L. Z., & Zhang, C. H. (2007). New idea of the Meso- and Neoproterozoic chronostratigraphic chart and tectonic environment in Sino-Korean Plate. *Geol.Bull. China*, *26*, 503–509. (in Chinese with English abstract)

Reinhard, C. T., Planavsky, N. J., Gill, B. C., Ozaki, K., Robbins, L. J., Lyons, T. W., et al. (2017). Evolution of the global phosphorus cycle. *Nature*, *541*, 386–389. http://doi.org/10.1038/nature20772

Reinhard, C. T., Planavsky, N. J., Olson, S. L., Lyons, T. W., & Erwin, D. H. (2016). Earth's oxygen cycle and the evolution of animal life. *Proceedings of the National Academy of Sciences*, *113*, 8933–8938. http://doi.org/10.1073/pnas.1521544113

Reinhard, C. T., Planavsky, N. J., Robbins, L. J., Partin, C. A., Gill, B. C., Lalonde, S. V., et al. (2013). Proterozoic ocean redox and biogeochemical stasis. *Proceedings of the National Academy of Sciences*, *110*(14), 5357–5362. http://doi.org/10.1073/pnas.1208622110

Reinhard, C. T., Planavsky, N. J., Ward, B. A., Love, G. D., Le Hir, G., & Ridgwell, A. (2020). The impact of marine nutrient abundance on early eukaryotic ecosystems. *Geobiology*, *18*, 139–151. http://doi.org/10.1111/gbi.12384

Robbins, L. J., Lalonde, S. V., Planavsky, N. J., Partin, C. A., Reinhard, C. T., Kendall, B., et al. (2016). Trace elements at the intersection of marine biological and geochemical evolution. *Earth-Science Reviews*, *163*, 323–348. http://doi.org/10.1016/j.earscirev.2016.10.013

Robinson, R. S., Kienast, M., Albuquerque, A. L., Altabet, M., Contreras, S., Holz, R. D. P., et al. (2012). A review of nitrogen isotopic alteration in marine sediments. *Paleoceanography*, *27*(4), 89–108. http://doi.org/10.1029/2012pa002321

Sahoo, S. K., Planavsky, N. J., Kendall, B., Wang, X., Shi, X., Scott, C., et al. (2012). Ocean oxygenation in the wake of the Marinoan glaciation. *Nature*, *489*(7417), 546–549. http://doi.org/10.1038/nature11445

Scholz, F. (2018). Identifying oxygen minimum zone-type biogeochemical cycling in Earth history using inorganic geochemical proxies. *Earth-Science Reviews*, *184*, 29–45. https://doi.org/10.1016/j.earscirev.2018.08.002

Scott, C., & Lyons, T. W. (2012). Contrasting molybdenum cycling and isotopic properties in euxinic versus non-euxinic sediments and sedimentary rocks: Refining the paleoproxies. *Chemical Geology*, *324–325*, 19–27. http://doi.org/10.1016/j.chemgeo.2012.05.012

Scott, C., Lyons, T. W., Bekker, A., Shen, Y. A., Poulton, S. W., Chu, X. L., & Anbar, A. D. (2008). Tracing the stepwise oxygenation of the Proterozoic ocean. *Nature*, *452*(7186), 456–459. http://doi.org/10.1038/nature06811

Shang, M., Tang, D., Shi, X., Zhou, L., Zhou, X., Song, H., & Jiang, G. (2019). A pulse of oxygen increase in the early Mesoproterozoic ocean at ca. 1.57–1.56 Ga. *Earth and Planetary Science Letters*, 527. https://doi.org/10.1016/j.epsl.2019.115797

Sheen, A. I., Kendall, B., Reinhard, C. T., Creaser, R. A., Lyons, T. W., Bekker, A., et al. (2018). A model for the oceanic mass balance of rhenium and implications for the extent of proterozoic ocean anoxia. *Geochimica et Cosmochimica Acta*, *227*, 75–95. https://doi.org/10.1016/j.gca.2018.01.036

Shi, M., Feng, Q., Khan, M. Z., & Zhu, S. (2017). An eukaryote-bearing microbiota from the early Mesoproterozoic Gaoyuzhuang Formation, Tianjin, China and its significance. *Precambrian Research*, *303*, 709–726. https://doi.org/10.1016/j.precamres.2017.09.013

Sigman, D. M., Karsh, K. L., & Casciotti, K. L. (2009). Ocean process tracers: Nitrogen isotopes in the ocean. In *Encyclopedia of ocean science*, (pp. 4138–4153). Amsterdam: Elsevier.

Slack, J. F., Grenne, T., Bekker, A., Rouxel, O. J., & Lindberg, P. A. (2007). Suboxic deep seawater in the late Paleoproterozoic: Evidence from hematitic chert and iron formation related to seafloor-hydrothermal sulfide deposits, central Arizona, USA. *Earth and Planetary Science Letters*, *255*, 243–256. https://doi.org/10.1016/j.epsl.2006.12.018

Sperling, E. A., Rooney, A. D., Hays, L., Sergeev, V. N., Vorob'Eva, N. G., Sergeeva, N. D., et al. (2014). Redox heterogeneity of subsurface waters in the Mesoproterozoic ocean. *Geobiology*, *12*, 373–386. http://doi.org/10.1111/gbi.12091

Sperling, E. A., Wolock, C. J., Morgan, A. S., Gill, B. C., Kunzmann, M., Halverson, G. P., et al. (2015). Statistical analysis of iron geochemical data suggests limited late Proterozoic oxygenation. *Nature*, *523*(7561), 451–454. http://doi.org/10.1038/nature14589

Stüeken, E. E. (2013). A test of the nitrogen-limitation hypothesis for retarded eukaryote radiation: Nitrogen isotopes across a Mesoproterozoic basinal profile. *Geochimica et Cosmochimica Acta*, *120*, 121–139. http://doi.org/10.1016/j.gca.2013.06.002

Stüeken, E. E., Kipp, M. A., Koehler, M. C., & Buick, R. (2016). The evolution of Earth's biogeochemical nitrogen cycle. *Earth-Science Reviews*, *160*, 220–239. http://doi.org/10.1016/j.earscirev.2016.07.007

Stüeken, E. E., Zaloumis, J., Meixnerová, J., & Buick, R. (2017). Differential metamorphic effects on nitrogen isotopes in kerogen extracts and bulk rocks. *Geochimica et Cosmochimica Acta*, *217*, 80–94. https://doi.org/10.1016/j.gca.2017.08.019

Su, W. (2014). A review of the revised Precambrian time scale (GTS2012) and the search of the Mesoproterozoic chronostratigraphy of China. *Earth Science Frontiers*, *21*(2), 119–138. (in Chinese with English abstract)
Tang, D., Shi, X., Wang, X., & Jiang, G. (2016). Extremely low oxygen concentration in mid-Proterozoic shallow seawaters. *Precambrian Research*, *276*, 145–157. http://doi.org/10.1016/j.precamres.2016.02.005
Tang, D., Shi, X., Zhang, W., Liu, Y., & Wu, J. (2017). Mesoproterozoic herringbone calcite from North China Platform: Genesis and paleoenvironmental significance. *Journal of Palaeogeography*, *19*(2), 227–240. (in Chinese with English abstract)
Taylor, S.R., & McLennan, S.M., (1985). The continental crust: Its composition and evolution. Blackwell, Oxford (312 pp.).
Tesdal, J. E., Galbraith, E. D., & Kienast, M. (2013). Nitrogen isotopes in bulk marine sediment: Linking seafloor observations with subseafloor records. *Biogeosciences*, *10*(1), 101–118. http://doi.org/10.5194/bg-10-101-2013
Thomazo, C., Ader, M., & Philippot, P. (2011). Extreme ^{15}N-enrichments in 2.72-Gyr-old sediments: Evidence for a turning point in the nitrogen cycle. *Geobiology*, *9*(2), 107–120. http://doi.org/10.1111/j.1472-4669.2011.00271.x
Thomazo, C., & Papineau, D. (2013). Biogeochemical cycling of nitrogen on the early Earth. *Elements*, *9*(5), 345–351. http://doi.org/10.2113/gselements.9.5.345
Thunell, R. C., Sigman, D. M., Muller-Karger, F., Astor, Y., & Varela, R. (2004). Nitrogen isotope dynamics of the Cariaco Basin, Venezuela. *Global Biogeochemical Cycles*, *18*(3), GB3001. http://doi.org/10.1029/2003gb002185
Tian, H., Zhang, J., Li, H. K., Su, W. B., Zhou, H. Y., Yang, L. G., et al. (2015). Zircon LA-MC-ICPMS U-Pb dating of tuff from Mesoproterozoic Gaoyuzhuang Formation in Jixian County of North China and its geological significance. *Acta Geoscientica Sinica*, *36*(5), 647–658.
Tribovillard, N., Algeo, T. J., Baudin, F., & Riboulleau, A. (2012). Analysis of marine environmental conditions based on molybdenum–uranium covariation—Applications to Mesozoic paleoceanography. *Chemical Geology*, *324–325*, 46–58. http://doi.org/10.1016/j.chemgeo.2011.09.009
Tribovillard, N., Algeo, T. J., Lyons, T., & Riboulleau, A. (2006). Trace metals as paleoredox and paleoproductivity proxies: An update. *Chemical Geology*, *232*(1), 12–32. http://doi.org/10.1016/j.chemgeo.2006.02.012
Wang, D., Ling, H. F., Struck, U., Zhu, X. K., Zhu, M., He, T., et al. (2018). Coupling of ocean redox and animal evolution during the Ediacaran-Cambrian transition. *Nature Communications*, *9*(1), 2575. http://doi.org/10.1038/s41467-018-04980-5
Wang, X., Jiang, G., Shi, X., Peng, Y., & Morales, D. C. (2018). Nitrogen isotope constraints on the early Ediacaran ocean redox structure. *Geochimica et Cosmochimica Acta*, *240*, 220–235. https://doi.org/10.1016/j.gca.2018.08.034
Wang, X., Shi, X., Tang, D., & Zhang, W. (2013). Nitrogen isotope evidence for redox variations at the Ediacaran-Cambrian transition in South China. *Journal of Geology*, *121*(5), 489–502. http://doi.org/10.1086/671396
Wei, H., Wang, X., Shi, X., Jiang, G., Tang, D., Wang, L., & An, Z. (2019). Iodine content of the carbonates from the Doushantuo Formation and shallow ocean redox change on the Ediacaran Yangtze Platform, South China. *Precambrian Research*, *322*, 160–169. https://doi.org/10.1016/j.precamres.2019.01.007
Xu, D., Wang, X., Shi, X., Tang, D., Zhao, X., Feng, L., & Song, H. (2020). Nitrogen cycle perturbations linked to metazoan diversification during the early Cambrian. *Palaeogeography, Palaeoclimatology, Palaeoecology*, *538*, 109392. https://doi.org/10.1016/j.palaeo.2019.109392
Yang, J., Junium, C. K., Grassineau, N. V., Nisbet, E. G., Izon, G., Mettam, C., et al. (2019). Ammonium availability in the Late Archaean nitrogen cycle. *Nature Geoscience*, *12*, 553–557. http://doi.org/10.1038/s41561-019-0371-1
Yang, S., Kendall, B., Lu, X., Zhang, F., & Zheng, W. (2017). Uranium isotope compositions of mid-Proterozoic black shales: Evidence for an episode of increased ocean oxygenation at 1.36 Ga and evaluation of the effect of post-depositional hydrothermal fluid flow. *Precambrian Research*, *298*, 187–201. https://doi.org/10.1016/j.precamres.2017.06.016
Zegeye, A., Bonneville, S., Benning, L. G., Sturm, A., Fowle, D. A., Jones, C., et al. (2012). Green rust formation controls nutrient availability in a ferruginous water column. *Geology*, *40*, 599–602. http://doi.org/10.1130/g32959.1
Zerkle, A. L., Poulton, S. W., Newton, R. J., Mettam, C., Claire, M. W., Bekker, A., & Junium, C. K. (2017). Onset of the aerobic nitrogen cycle during the great oxidation event. *Nature*, *542*(7642), 465–467. http://doi.org/10.1038/nature20826
Zhang, K., Zhu, X., Wood, R. A., Shi, Y., Gao, Z., & Poulton, S. W. (2018). Oxygenation of the mesoproterozoic ocean and the evolution of complex eukaryotes. *Nature Geoscience*, *11*(5), 345–350. http://doi.org/10.1038/s41561-018-0111-y
Zhang, S., Wang, X., Wang, H., Bjerrum, C. J., Hammarlund, E. U., Costa, M. M., et al. (2016). Sufficient oxygen for animal respiration 1,400 million years ago. *Proceedings of the National Academy of Sciences*, *113*(7), 1731–1736. http://doi.org/10.1073/pnas.1523449113
Zhang, X., Sigman, D. M., Morel, F. M. M., & Kraepiel, A. M. L. (2014). Nitrogen isotope fractionation by alternative nitrogenases and past ocean anoxia. *Proceedings of the National Academy of Sciences*, *111*(13), 4782–4787. http://doi.org/10.1073/pnas.1402976111
Zhu, S., Zhu, M., Knoll, A. H., Yin, Z., Zhao, F., Sun, S., et al. (2016). Decimetre-scale multicellular eukaryotes from the 1.56-billion--year-old Gaoyuzhuang Formation in North China. *Nature Communications*, *7*, 11500. http://doi.org/10.1038/ncomms11500